

# **Functional Electrospun Nanofiber Coating on Metal and Polymer Implants**

**By**

**Subhakar Tummala**

Master of Science in Engineering Physics-Mechanical Engineering

University of Central Oklahoma

Edmond, Oklahoma

2018

Master Thesis

Submitted to the Faculty of

The Graduate College of the University of Central Oklahoma

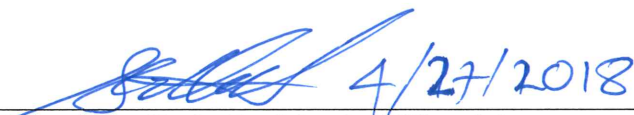
In partial fulfillment of the requirements for the Degree of

Master of Science in Engineering Physics- Mechanical Engineering

May 2018.

# Functional Electro Spun Nanofiber Coating on Metal and Polymer Implants

Thesis Approved:

  
4/27/2018

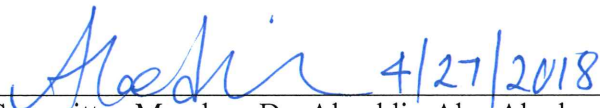
---

Committee Chair: Dr. Morshed Khandaker

  
4/27/2018

---

Committee Member: Dr. Mohammad Hossan

  
4/27/2018

---

Committee Member: Dr. Alaeddin Abu-Abed

## ACKNOWLEDGMENTS

I would like to express my deepest sense of appreciation to my advisor, Dr. Morshed Khandaker, for the continuous support of my master study and research, for his patience, motivation, enthusiasm, and immense knowledge. His guidance helped me in all the time of research and writing of this thesis. I could not have imagined having a better advisor and mentor for my master study.

I am thankful to my committee members, Dr. Mohammad Hossan and Dr. Alaeddin Abu-Abed for their encouragement, insightful comment, and support during my research.

I am also indebted to the Department of Engineering and Physics, the College of Mathematics and Science, and the Graduate College at the University of Central Oklahoma.

I would like to thank my professors during the graduate studies and my research mates for their cooperation and guidance.

Finally, I take this opportunity to express profound gratitude from the deep of my heart to my beloved parents Venkateswara Rao Tummala and Suseela Tummala for their continuous love and support. I also thank my uncle Dr. Sai (Giridhar) Tummala and my aunt Dr. Rama Tummala for their continuous motivation and support throughout.

## Abstract

Electrospun nanofiber is used for wide range of applications in the field of biomedical engineering because of its ease of production. Due to its low cost, biocompatibility, and slow bio resorption, poly- $\epsilon$ -caprolactone (PCL) is used as a polymer to produce the nanofiber for various applications. The main goal of this thesis is to use electrospun nanofiber to improve the biological efficiency of the polymer and metal implants. There are three independent objectives achieved in this thesis.

To achieve the first objective, the biomechanical performances of the intervertebral disc (IVD) implant anchored with electrospun nanofiber mesh to the natural and those IVDs made with silicone NP only are compared. The compression and the rheological test results show that ENAS disc compressive modulus is significantly higher in comparison to silicone gel. These values are in the range of native human IVD.

To achieve the second objective, the laser grooved titanium implant is treated with tesryl chloride and fibernectin and is coated with PCL nanofibers to use as an implant for the femur of a rabbit. After the Histological analysis, it is observed that the Osseointegration of the implant is increasing with time.

For the third objective, a preliminary study has been carried out to see if we can fabricate a blood vessel implant using Nylon-6. A simulated blood fluid is passed through the blood vessel and the flow test, rupture test, and tensile tests are conducted. It is concluded that Nylon-6 is a potential substitute to fabricate a blood vessel.

## Table of Contents

1. INTRODUCTION _____	11
1.1. Electrospinning: _____	11
1.2 Materials investigated in the study: _____	12
1.2.1 Titanium _____	12
1.2.2 Polycaprolactone _____	12
1.2.3 Silicone Gel _____	12
1.2.4 PEGDA _____	13
1.3 Motivation and goals _____	14
1.4 Objectives _____	14
1.5 Organization of the thesis _____	15
2. EVALUATION OF BIOMECHANICAL PERFORMANCES OF AN ELECTROSPUN NANOFIBER ANCHORED SILICONE DISC AS AN INTERVERTEBRAL DISC IMPLANT _____	16
2.1 Summary: _____	16
2.2 Background and Significance: _____	17
2.3 Materials and Methods: _____	19
2.3.1 Specimen preparation: _____	19
2.3.2 Compression Tests: _____	20
2.3.3 Rheological tests: _____	21
2.3.4 Histological Analysis: _____	21
2.3.5 Finite Element model _____	22
2.4 Results and Discussion _____	25
2.4.1 Compression Test: _____	25
2.4.2 Rheological Test: _____	26

2.4.3	Finite Element Analysis:	_____	27
2.4.4	Disc Heights:	_____	31
2.5	Conclusion:	_____	33
2.6	Acknowledgements:	_____	34
2.7	Future Works:	_____	34
3.	THE IN-VIVO BIOLOGICAL RESPONSE OF NANOFIBER COATING ON A METAL IMPLANT	_____	35
3.1	Summary	_____	35
3.2	Background and Significance	_____	36
3.3	Materials and Methods	_____	37
3.4	Results and Discussions	_____	41
3.4.1	Histological Analysis	_____	41
3.4.2	Bone formation and resorption:	_____	42
3.4.3	$\mu$ CT analysis:	_____	43
3.5	Conclusion:	_____	44
3.6	Acknowledgments:	_____	44
3.7	Future Works:	_____	44
4.	DESIGN AND FABRICATION OF A BLOOD VESSEL	_____	45
4.1	Summary:	_____	45
4.2	Background and Significance:	_____	45
4.3	Materials and Methods:	_____	46
4.4	Results and Discussion:	_____	47
4.4.1	Flow Test:	_____	47
4.4.2	Rupture test:	_____	48
4.4.3	Tensile Test:	_____	48

4.4.4 ANSYS Simulation:	50
4.5 Conclusion:	51
4.6 Acknowledgements:	51
4.7 Future Works:	51

## List of Figures

Figure 1-1 Schematic of electrospinning set up.....	11
Figure 2-1: Annulus Fibrosus and Nucleus Pulposus inside an IVD. [10].....	17
Figure 2-2: Schematic representation of 6 DOF's of an IVD. [12] .....	18
Figure 2-3: An ENAS Disc.....	21
Figure 2-4: 3D CAD Model of Spine .....	23
Figure 2-5: Components of Spine Disc.....	23
Figure 2-6: Finite Element Mesh Model of Spine Disc.....	25
Figure 2-7: Load vs. displacement curve of an ENAS disc from a compression test.....	26
Figure 2-8 (a) Rheological test results of Silicone Disc .....	27
Figure 2-8 (b): Rheological test results of ENAS disc .....	27
Figure 2-9: FEA Results for natural NP .....	28
Figure 2-10: CT scan images showing the Rat tails 1(a), 1(b) and 1(c) on the left and the rat tails 2(a), 2(b) and 2(c) to the right.....	31
Figure 2-11: (a) front (b) rear and (c) side view of the rat tail IVD implant .....	32
Figure 3-1: (a) Laser grooving on the Ti surface using Full Spectrum Laser (b) SEM image of the implant .....	37
Figure 3-2: The modified Ti samples are coated with PCL nanofibers, placed in a holder. ....	38
Figure 3-3: The implant is embedded in the Technovit-7200 VLC.....	39
Figure 3-4: The sample is sandwiched between a thick and thin plastic slide. ....	40
Figure 4-5: The cell growth is counted in the highlighted area .....	41



Figure 3-6: Showing the cell growth after (a) 14 days (b) 28 days (c) 42 days after implantation .....	42
Figure 3-7: Amount of OC, ALP, and TRAP present in the serum concentration over a period of implantation.....	43
Figure 3-8: Graph plotted for mean voxel value for period of implantation. ....	43
Figure 4-1: Blood vessel fabricated by Nylon-6.....	46
Figure 4-2: A mini variable Flow Pump.....	47
Figure 4-3: Flow test setup for a fabricated blood vessel.....	48
Figure 4-4: (a) The blood vessel is fixed between two jaws of the Test Resources machine (b) Breaking of the fabricated blood vessel.....	49
Figure 4-5: Graph plotted to determine tensile strength with Time(s) on X-axis and Load (N) and Stroke (mm) on Y-axis .....	49
Figure 4-6: The contours of (a) Pressure and (b) Velocity of a simulated blood vessel...	51

## **List of tables**

Table 2-1: Material properties used in the analysis _____	24
Table 2-2: Maximum Stress results for Natural Disc _____	29
Table 2-3. Maximum Stress Results for Silicone Disc _____	30
Table 2-4: Maximum Stress Results for ENAS Disc _____	31
Table 2-5(a): Disc heights of the implanted IVD _____	32
Table 2-5(b): Disc heights of SHAM IVD _____	33



## **1.2 Materials investigated in the study:**

### **1.2.1 Titanium**

Titanium (Ti) based alloy have been widely used in orthopedic and orthodontic surgeries as implants because of their strong mechanical, chemical (corrosion resistance), and biological properties and biocompatibility. [1] In this particular study, Ti-6AL-4V was used as it is the most widely used material for implants because of its better physical and mechanical properties compared to pure Ti.

A depth of 100-micron size grooves was created on the 2.2mm diameter Ti rod using Full spectrum laser machine to analyze the effect of surface modification on a titanium implant on the cell growth.

### **1.2.2 Polycaprolactone**

Due to its low cost, biocompatibility, and slow bio resorption, poly- $\epsilon$ -caprolactone (PCL) is used as a polymer to produce the nanofiber for various applications. PCL is a versatile polymer and is used in various long-term biodegradation biomaterials. A low degradation of 3-4 years makes PCL more suitable for long-term degrading implants and applications. The distinct rheological and viscoelastic properties of PCL and the ease to produce nanofibers makes PCL as a widely used biomaterial. [2] It is also used in drug delivery devices which are approved by Food and Drug Administration (FDA).

### **1.2.3 Silicone Gel**

Hydrogels are very promising in the field of biomedical engineering due to their unique properties like high water content, softness, flexibility and biocompatibility.

Hydrophilic polymers can be physically or chemically cross-linked in order to produce hydrogels. Hydrogels are used in tissue engineering, contact lenses, implantations and in the drug delivery systems. [3, 4] Silicone gel is one of the widely used polymer gel as an implant and is a perfect hydrogel which mimics the Nucleus Pulposus (NP) of an Intervertebral Disc (IVD). It is prepared by mixing polydimethylvinylsiloxane and polydimethylhydrogensiloxane in equal weight ratio.

#### 1.2.4 PEGDA

Tissue engineering (TE) holds great promise for the cultivation of patient-specific tissues for restoring organ functions and/or curing various diseases. [5] Photosensitive hydrogels, such as Poly Ethylene Glycol Di Acrylate (PEGDA) are an important class of biomaterials with many TE applications. [6, 7] Photolithography is a commonly used process in micro-fabrication to produce the desired scaffold with specific shape and size using a mold. [8] The ability to control the porosity of photosensitive hydrogel such as Poly Ethylene Glycol Di Acrylate (PEGDA) to elicit altered cell behaviors, including cell adhesion, has raised heightened interest in the scaffold materials for various biomedical applications such as orthopedic repair and regeneration [6] and liver tissue engineering. [9] This material study focuses on the physical, mechanical and biological capabilities of PEDGA-PCL scaffold and evaluates the capabilities for tissue engineering applications.

### 1.2.5 Nylon-6

To obtain a higher tensile strength with biocompatibility and should not degrade quickly, Nylon-6 will be the best choice. It is biocompatible and non-biodegradable with higher tensile strength. It can also be produced by electrospinning method. The nanofiber polymer solution is prepared by mixing the Nylon-6 in 88% Formic Acid, which is a class 3 solvent and is approved by the Food and Drug Administration.

## 1.3 Motivation and goals

The motivation of this thesis was to evaluate the effect of the coating of the PCL nanofibers on different materials: Micro-grooved Titanium implants, Silicone hydrogel implant and a fabricated blood vessel using PCL. The goals were to measure the effect of PCL nanofibers on Ti implants, Silicone gel implant by conducting in-vivo and in-vitro tests and to test the maximum flow rate of a blood vessel fabricated by PCL.

## 1.4 Objectives

The objectives of this thesis are 1) To determine the effect of bone growth on a nanofiber coated, micro-grooved titanium implant 2) To increase the mechanical strength of an intervertebral disc implant by anchoring it with the PCL electrospun nanofibers 3) Fabricate and test the flow of a PCL blood vessel.

## **1.5 Organization of the thesis**

This thesis contains six chapters. Chapter 1 is the introduction of the thesis. In Chapter 2, the biomechanical performances of an electrospun anchored silicone disc as an intervertebral disc implant has been evaluated. Chapter 3 was to evaluate the in vivo effects of the PCL ENF coating on the surface topography of a titanium implant by histological analysis. In chapter 4, the preliminary study to produce a blood vessel PCL in a novel process has been done.

## CHAPTER 2

### 2. EVALUATION OF BIOMECHANICAL PERFORMANCES OF AN ELECTROSPUN NANOFIBER ANCHORED SILICONE DISC AS AN INTERVERTEBRAL DISC IMPLANT

#### 2.1 Summary:

Millions of people are suffering from disc degenerative disease. Nucleus Pulposus (NP), a jelly-like structure inside intervertebral disc (IVD), is losing its water content due to the disease. As a result, the six degrees of freedoms (DOF's) of a spine, consisting of flexion, extension, compression, laterolateral shear, anteroposterior shear and axial rotation are lost. Our ex vivo study using rabbit tail model found that silicone is able to mimic the mechanical properties of NP, but it fails to maintain the disc stability. Tissue engineered intervertebral disc (IVD) anchor the circumference and top/bottom sides of Nucleus Pulposus (NP) implants with annulus fibrosus and endplates. [10] The proper anchorage of an NP implant to annulus fibrosus and endplates is possible by enclosing the NP by electrospun fiber mesh that mimics the surrounding structures. The biomechanical performance of silicone-based NP can be improved if electrospun fiber mesh can secure all sides of silicone NP. This study compared the compressive and viscoelastic properties of a silicone and electrospun nanofiber anchored silicone discs (ENAS) under compression and shear with the same properties of human NP. This study also developed a nonlinear finite element model (FEM) for the intact and ENAS implanted human lumbar vertebra segments. The compression test results show that ENAS disc compressive modulus ( $87.47 \pm 7.56$  kPa,  $n = 3$ ) is significantly higher in comparison to silicone gel ( $38.75 \pm 2.15$  kPa,  $n = 3$ ) and the value is within the range of the compressive modulus of human NP ( $64.9 \pm$



44.1 kPa). The rheological test results show that ENAS disc compressive modulus (16 ~ 40 kPa) is significantly higher in comparison to silicone gel (0.10 ~ 0.16 kPa) and the value is within the range of the compressive modulus of human NP (7 ~ 20 kPa). These results confirm the suitability of the ENAS disc over the silicone as NP implant. A finite element model has been developed based on the ENAS properties. The FEA results showed that ENAS can restore better the biomechanical motions of lumbar vertebra segments in compare to silicone NP.

## **2.2 Background and Significance:**

Millions of people are suffering from disc degenerative disease. Due to this, Nucleus Pulposus (NP), a jelly like structure inside the intervertebral disc (IVD) is losing its water content and as a result the 6 DOF's by NP are lost. An intervertebral disc is an anatomical structure that is sandwiched between two vertebrae in the spine. The IVD consists of a core, or Nucleus Pulposus, surrounded by a fibrous covering known as the annulus fibrosus as shown in the Figure 2-1.

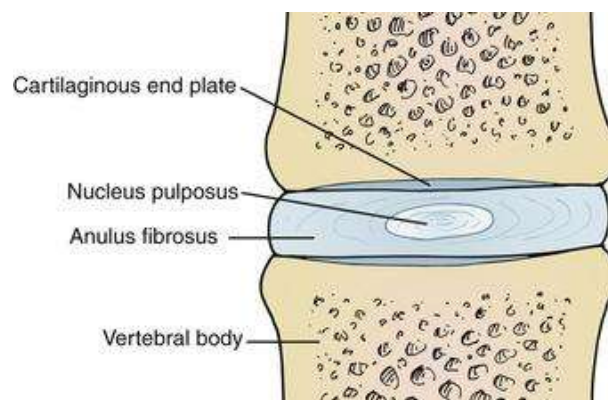


**Figure 2-1: Annulus Fibrosus and Nucleus Pulposus inside an IVD. [11]**

The IVD acts as a shock absorber for the spine, in addition to enabling six degrees of freedom (6 DOF) motions, consisting of flexion, extension, right and left lateral bending, compression, and axial rotation as shown in Figure 2-2.

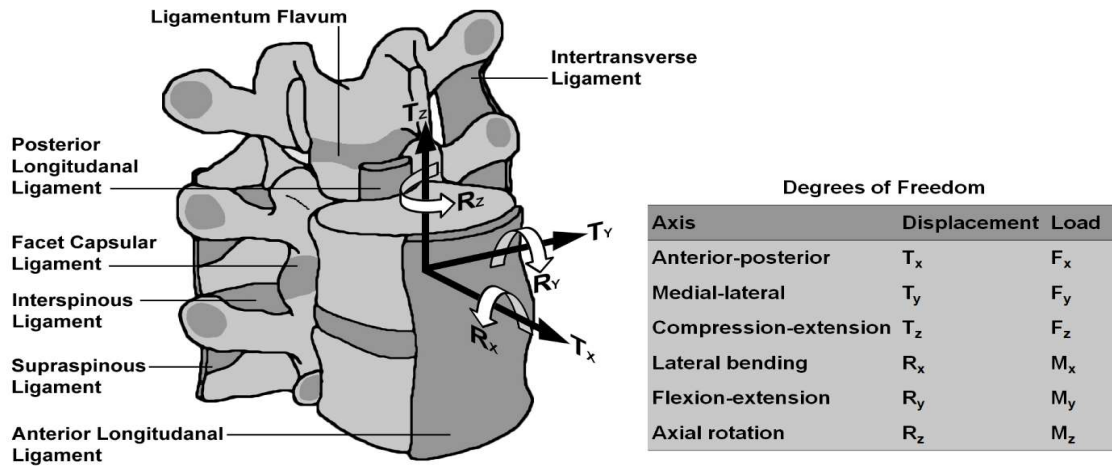


**Figure 2-2: Schematic representation of 6 DOF's of an IVD. [12]**

One cause of degenerative disc disease is the deterioration of the Nucleus Pulposus, generally due to dehydration. One method of addressing this form of degenerative disc disease is to implant a replacement Nucleus Pulposus. These replacements can consist of ceramics, polymers, or metals. A functional IVD replacements material and implantation technique must restore the biomechanical functions of the disc after implantation. [13] In order to obtain a biomechanical equivalent natural IVD, it requires proper anchoring of the NP implants and its replacement inside the disc. Such anchorage may restore the disc stability after discectomy. Electrospun fibers are commonly exploited as tissue engineering scaffold because of their ability to mimic natural tissues. However, their clinical use remains restricted due to negligible cellular infiltration and poor mechanical properties. [7] A small number of research

groups investigated composite scaffolds based on electrospun fibers for IVD applications. [14] [13] [15] [16] The electrospinning process can produce angle-ply structures that recreate the organized fibrous architecture of the native AF. [15] Single strip of the aligned scaffold can be arranged concentrically, precisely mimicking the alternating fiber alignment of native tissue, to form disc-like angle-ply structures. [13] The study shows these constructs mature both compositionally and mechanically over time in culture, indicating their potential for use in total disc replacement. But there is no electrospun fiber production technique developed till today to anchor all sides of NP implant by fiber mesh. Such anchorage can satisfy the long-term biomechanical functions requirement of an IVD. Khandaker and Shahram [17] developed a novel electrospun fiber production technique (patent pending) to anchor NP gels by aligned electrospun fiber mesh that also can act as AF and EP scaffolds. This study investigated whether the biomechanical performance of IVDs having electrospun AF and EP fiber mesh is comparable to those IVDs made with silicone NP only. This study measured the mechanical responses from intact and implanted human vertebral specimens using a finite element modeling under 6 DOF spine motions.

## **2.3 Materials and Methods:**

### **2.3.1 Specimen preparation:**

An electrospun fiber machine was used to produce the EIVD. The PCL acetone polymer solution used in the fiber production. The solution was prepared using a 92.3% to 7.7% by weight ratio of acetone and PCL, respectively. The dimension of gel and fiber layers in the EIVD is equipment to the NP and AF dimension of a rabbit tail at caudal

disc 4 (found from CT image of a rabbit tail). A hollow shaft (outside diameter same as the rabbit nucleus diameter) was mounted on a linear motorized stage. The stage was programmed to provide stepwise linear translation and rotational motion to the shaft at a 30° angle. An electrospun cloth and fiber cup was produced. A heated punch was used to cut a 1 mm diameter of fiber piece from the cloth. Silicone gel was prepared by mixing a 40 wt% of poly-dimethyl-hydrogen-siloxane crosslinker agent with the polydimethylvinylsiloxane base. [19] Both base and cross-linker were purchased from Applied Silicone Corporation. The silicone mixture was poured into an aluminum mold with wells having 1 mm diameter and 2 mm depth. The mold was placed into a vacuum chamber under pressure for 15 minutes to collapse bubbles in the mixture. This vacuum process was done four times. The pressure was released and the temperature increased to 165°C where the silicone cured for 3 hours. Silicone gel was carefully filled in the fiber cup, pressed, and then 1 mm diameter fiber piece was placed at the top of the gel. The extra fiber in the fiber cup above the top of the fiber piece was trimmed and glued the piece with the cup by a heated blunt needle.

### 2.3.2 Compression Tests:

Evex tension/compression test system was used to measure silicone NP and ENAS disc (Figure 2-3) gel mechanical behavior under compression. The gel was compressed to 80% of the gel height at a rate 0.05 mm/sec during the unconfined compression tests to determine the compressive modulus. The maximum compressive pressure of ENAS disc was measured from the load-displacement curve by applying pressure to the gel till breakage of the fiber layer.



**Figure 2-3: An ENAS Disc**

### 2.3.3 Rheological tests:

Viscoelastic properties of silicone and ENAS gels were measured using the Malvern CVO-100 rheometer at 1 Hz frequency (a typical oscillation rate of tissue in a rodent under motion). The viscoelastic properties of the polymer were obtained using a rheometer, which determined the elastic ( $G'$ ) and viscous ( $G''$ ) moduli of the silicone hydrogel polymer by calculating the complex shear modulus ( $G^*$ ) under low- frequency oscillating shear deformation.

### 2.3.4 Histological Analysis:

To determine the tissue formation around the implant, the IVD implants are implanted in a rat tail. A total of six rats are used in this experiment. Three rats are implanted with the engineered IVD which are anchored with PCL electrospun nanofibers and the other three rats are used for control. After 28 days, the rats are euthanized to collect the tails. Micro CT images are taken after the rats are euthanized and the disc heights are compared with the implanted to that of controlled ones. The samples are first decalcified using 0.05M Ethylenediaminetetraacetic acid (EDTA). Then the samples are

fixed in 10% phosphate-buffered formalin for 48 h. After fixation, the samples are washed with running water for a couple of hours and they are kept in 70% ethanol, 95% ethanol, and in three different solutions of absolute ethanol for 1 hour each. Then, the samples are embedded in paraffin wax and they are cut into thin sections of 8  $\mu\text{m}$  using a microtome. Sections are then stained with Safranin-O with Fast Green as a counterstain. Sections are stained with hematoxylin and eosin (H&E) to visualize cell infiltration and matrix deposition. Stained sections are observed and imaged under bright field with an upright microscope.

#### 2.3.5 Finite Element model

A Parasolid model of the L3 to L5 human vertebrae and IVDs (Figure 2-4) was purchased from Zygote Media Group in order to compare the results of the bovine tail to a human spine. The model was meshed and simulated using ANSYS Workbench. Finite element model is created for the spinal disc to understand, the effect of engineered silicone gel and ENAS disc effect on the stress values of the spine disc. Firstly the analysis is conducted for the natural Nucleus Pulposus then the natural NP is replaced with engineered silicone gel and ENAS disc respectively. The CAD model of the spine disc is created by using 3D scanning method. Then the model is modified in CATIA 3D-CAD software, the NP, annulus and endplate regions of the disc are created. The CAD model of the spine including L4, L5 vertebra, and one spinal disc is given in Figure 2-4 and the components of the single spinal disc are illustrated in Figure 2-5.

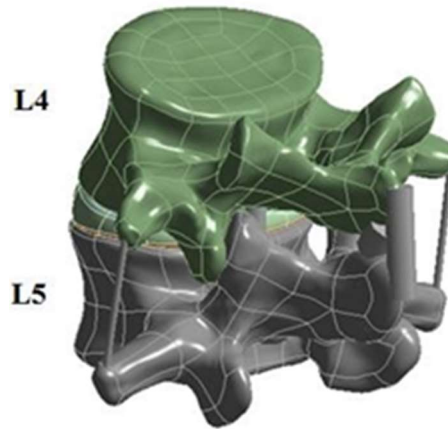


**Figure 2-4: 3D CAD Model of Spine**

After the definition of the CAD model of the spine, the CAD model is exported from CATIA to ANSYS V.14.

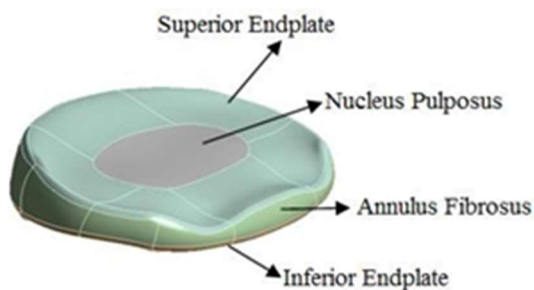


**Figure 2-5: Components of Spine Disc**

The FEA model is created a static structural module of the ANSYS software to find the stress distribution of the spine under different boundary conditions. The materials used in the finite element analysis is defined as an isotropic material. The model consists of three different parts, vertebra, disc, and ligaments the last part is engineered implants which are replaced with natural Nucleus Pulposus. Ligaments are defined as beam elements. The beam elements only work in the direction of tensile and compression. The materials properties which are used in the analysis are defined according to Shin *et al.* [18]. All materials properties used in the analysis are given in Table 2-1.

Material	Modulus of Elasticity (MPa)	Poisson Ratio	Cross-section (mm <sup>2</sup> )
<b>Vertebra</b>			
Cortical bone	12000	0.3	
Cancellous bone	100	0.2	
<b>Disc</b>			
Nucleus	1	0.499	
Annulus	8.4	0.45	
Endplate	24	0.4	
<b>Ligament</b>			
ALL	7.8	-	63.7
PLL	1	-	20
LF	1.5	-	40
TL	10	-	1.8
CL	7.5	-	30
IL	1	-	40
SL	3	-	30
<b>Engineered Implants</b>			
Silicone Gel	1.5	0.48	
Nanofiber Layer	30	0.49	

**ALL:** Anterior longitudinal ligament,

**PLL:** Posterior longitudinal ligament,

**LF:** Ligamentum flavum,

**TL:** Transverse ligament,

**CL:** Capsular ligament,

**IL:** Interspinous ligament,

**SL:** Supraspinous ligament.

**Table 2-1: Material properties used in the analysis**

The meshing process is one of the most important steps of the finite element analysis. The spine model is divided into meshes with different sizes. The mesh type is defined as a hexahedral mesh type and the mesh structure consists of both SOLID 187 and SOLID 186 mesh types. These mesh types are default mesh types of ANSYS workbench. The vertebra bodies mesh size is defined as 2mm and disc components meshes sizes are defined as 0.5 mm. Because the disc region should be more sensitive than the vertebral regions. The finite element mesh model of the spinal disc is shown in Figure 1-4. The mesh structure consists of approximately 160000 elements and 580000 nodes.



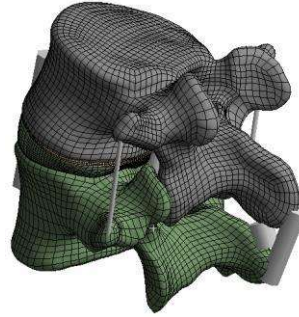


**Figure 2-6: Finite Element Mesh Model of Spine Disc**

One of the most difficult thing for the spine finite element analysis is to define boundary conditions of the system. In the literature many different boundary condition definition is available. In this study, the boundary conditions are defined according to Ueno *et al.*[19] Six different boundary conditions are applied to the spine model. The side surface of the L5 vertebral body is fully fixed in all directions. The loads are applied on the upper surface of the L4 vertebral body in the direction of extension, bending, and compression. These loads are the injury loads for a healthy human.

## **2.4 Results and Discussion**

### **2.4.1 Compression Test:**

The compression test results show that ENAS disc compressive modulus ( $87.47 \pm 7.56$  kPa,  $n = 3$ ) is significantly higher in comparision to silicone gel ( $38.75 \pm 2.15$  kPa,  $n = 3$ ) and the value is within the range of the compressive modulus of human NP ( $64.9 \pm 44.1$  kPa). The maximum compressive pressure of ENAS disc was measured from the load-displacement curve (Figure 2-7), which was 0.46 MPa. Since the range of resting compressive stress for animal tails is  $0.2 \pm 0.05$ MPa, therefore, our designed ENAS disc is adequate for the proposed study.

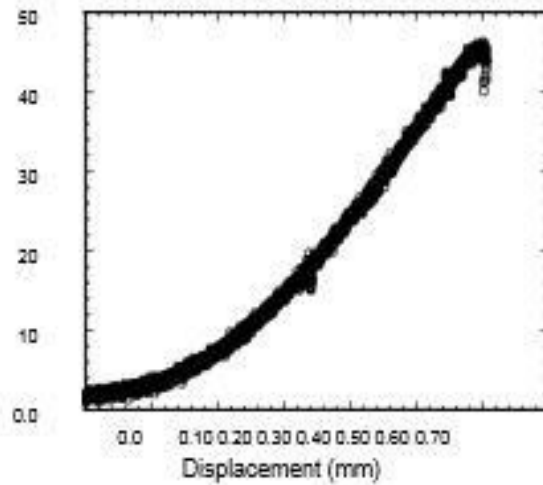
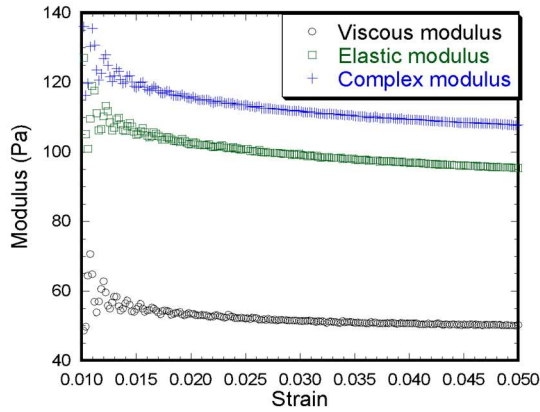


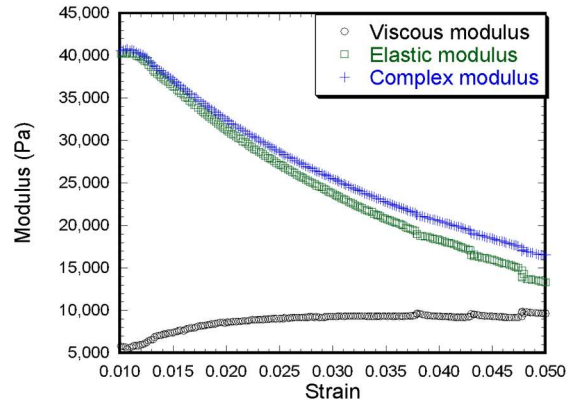
**Figure 2-7: Load vs. displacement curve of an ENAS disc from a compression test.**

#### 2.4.2 Rheological Test:

The rheological tests are conducted using a Malvern Rheometer. A small amount of sample is kept in the specimen chamber and the tests are carried out to determine the viscosity. The rheological test results (Figure 1-6) show that ENAS disc compressive modulus (16 ~ 40 kPa) is significantly higher in comparison to silicone gel (0.10 ~ 0.16 kPa) and the value is within the range of the compressive modulus of human NP (7 ~ 20 kPa). These results confirm the suitability of ENAS disc over silicone as NP implant.



(a)



(b)

**Figure 2-8 (a) Rheological test results of Silicone Disc**

**Figure 2-8 (b): Rheological test results of ENAS disc**

#### 2.4.3 Finite Element Analysis:

The results are obtained from the FE analysis under different loading conditions. The maximum Von-Misses stress results are taken into consideration. For the whole system, the maximum stress has occurred on the singular points of the vertebra between 30 MPa-21 MPa, these stress values are considerably lower than the cortical bone yield stress. Thus, for each analysis, the bones protect its durability. The average stress is taken nearly 5 MPa for each analysis. The stress distribution of the spine for each analysis on the natural spine is given in Figure 1-7.

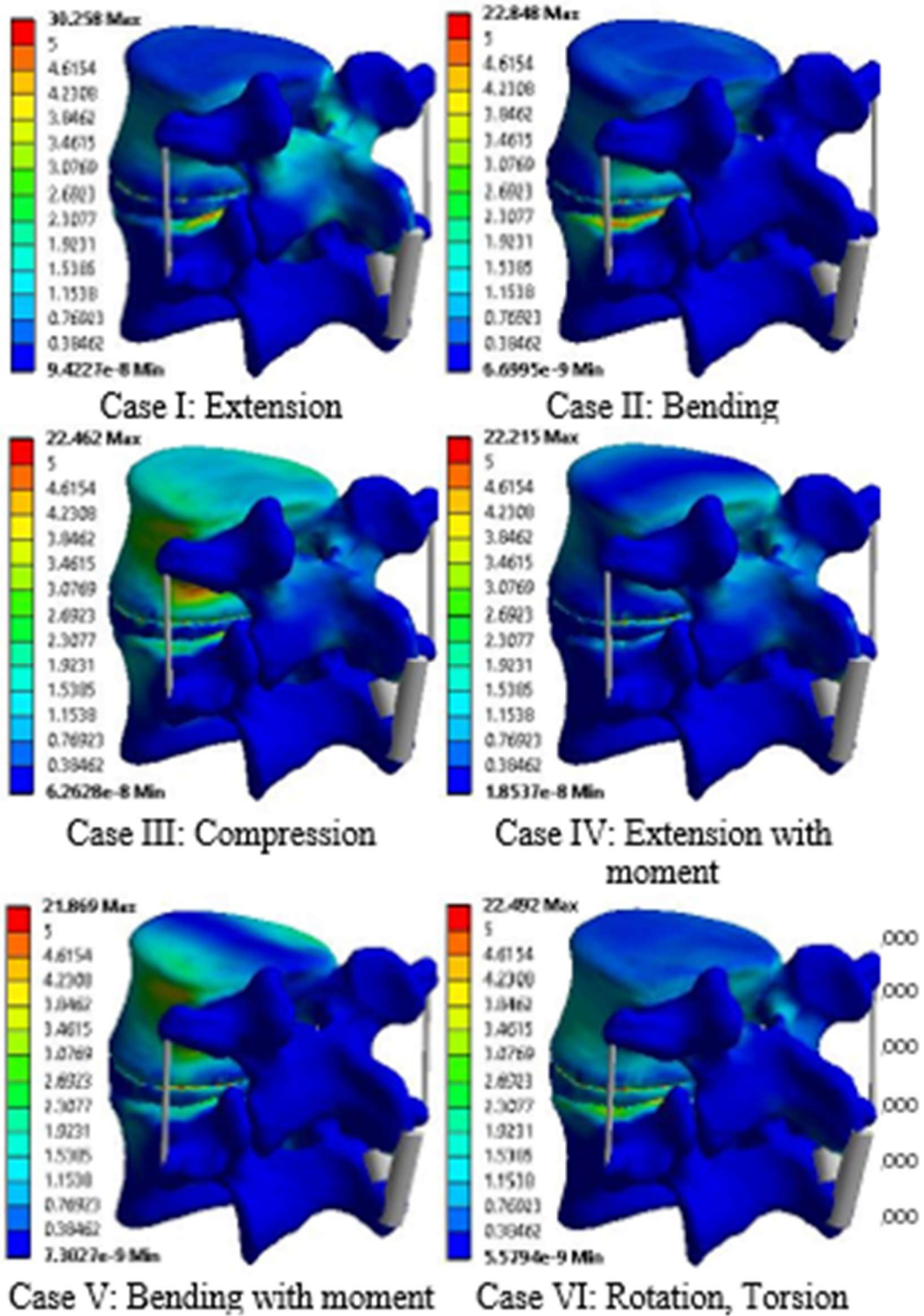


Figure 2-9: FEA Results for natural NP

Stress values which are occurred on the Nucleus Pulposus are the main interest of this study. Thus, the maximum stress values are taken from FEA for the NP. The first analysis is done with natural Nucleus Pulposus properties and it's seen that the stress values fluctuate between 1-1.8 MPa. These stress results are relatively high for the natural Nucleus Pulposus. For all cases, the stress results for NP is given in Table 2-2.

<b>Types of Experiments</b>	<b>Stress on the NP (MPa)</b>
<b>Case I: Extension</b>	1.032
<b>Case II: Bending</b>	1.649
<b>Case III: Compression</b>	1.556
<b>Case IV: Extension with moment</b>	1.223
<b>Case V: Bending with moment</b>	1.839
<b>Case VI: Rotation, Torsion</b>	1.252

**Table 2-2: Maximum Stress results for Natural Disc**

In the second analysis to understand engineered silicone gel performance, the natural NP properties are changed with engineered silicone gel properties. The other conditions are taken same with the first analysis and the analysis is run for the second time. When the natural NP, is changed with the silicone gel NP, the stress values are increased nearly two times. All results for the silicone gel is given in Table 2-3.

<b>Types of Experiments</b>	<b>Stress on the NP (MPa)</b>
<b>Case I: Extension</b>	1.457
<b>Case II: Bending</b>	2.041
<b>Case III: Compression</b>	2.382
<b>Case IV: Extension with moment</b>	2.357
<b>Case V: Bending with moment</b>	2.370
<b>Case VI: Rotation, Torsion</b>	2.407

**Table 2-3. Maximum Stress Results for Silicone Disc**

Finally, the natural NP is changed with the ENAS disc, also for the third time all boundary conditions are taken same. Only the natural NP properties are changed with the engineered properties. As a result of the third analysis, instead of silicone gel, the stress results are decreased with a comparison of the first analysis. The fiber layer thickness is taken 0.5 for this analysis. All results are given for the third analysis is given in Table 2-4. It's seen that the ENAS disc is the best fitting engineered NP for the spinal disc. The silicone gel is also fitted for the spine. The stress results can be said between acceptable levels.

Types of Experiments	Stress on the NP (MPa)
Case I: Extension	0.505
Case II: Bending	0.481
Case III: Compression	0.483
Case IV: Extension with moment	0.430
Case V: Bending with moment	0.543
Case VI: Rotation, Torsion	0.395

**Table 2-4: Maximum Stress Results for ENAS Disc**

#### 2.4.4 Disc Heights:

The IVD's are implanted in a rat tail to measure the impact on the disc heights. After 28 days of euthanization, the rat tails are recovered and CT images are taken to measure the change in the disc heights of the implanted and the sham IVD's. Sham IVD sample is where the native IVD is completely taken away. The CT scan images are shown in the Figure 1-8 below for the IVD implants and the SHAM tails.

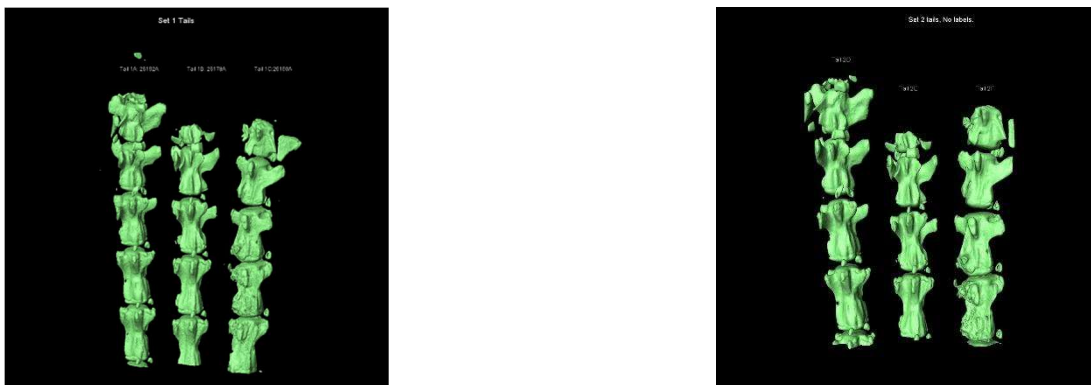


**Figure 2-10: CT scan images showing the Rat tails 1(a), 1(b) and 1(c) on the left and the rat tails 2(a), 2(b) and 2(c) to the right.**

The IVD implants are fabricated as per the dimensions of a rat's IVD. The diameter of the implant is 4mm with a thickness of 1mm as shown in the figure 1-9.

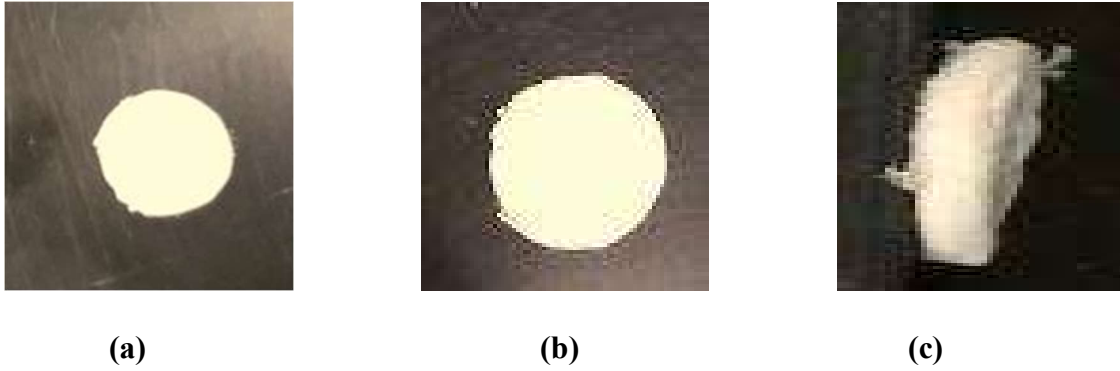


**Figure 2-11: (a) front (b) rear and (c) side view of the rat tail IVD implant**

The Disc heights of the IVD are calculated as shown in Table 2-5 below. Table 2-5 (a) shows the disc height calculation for the implanted IVD's and Table 2-5 (b) shows the disc height calculation for the SHAM IVD.

	1A		1B		1C	
View	Top	Bottom	Top	Bottom	Top	Bottom
XZ	0.76	0.46	0.73	0.52	0.64	1.12
	0.88	0.48	0.67	0.62	0.77	1.27
	1.08	0.64	0.81	0.64	0.85	1.09
	0.92	0.52	0.60	0.39	0.59	0.92
	0.94	0.52	0.28	0.43	0.69	0.92
YZ	0.78	0.46	0.60	0.63	0.53	0.83
	0.97	0.50	0.66	0.76	0.67	1.05
	1.01	0.70	0.78	0.77	0.88	1.02
	0.90	0.61	0.62	0.76	0.49	0.62
	0.95	0.62	0.60	0.73	0.41	0.73
Average	0.92	0.55	0.64	0.63	0.65	0.96

**Table 2-5(a): Disc heights of the implanted IVD**



	2D		2E		2F	
View	Top	Bottom	Top	Bottom	Top	Bottom
XZ	0.92	0.55	0.49	0.59	0.08	0.06
	0.78	0.52	0.68	0.67	0.02	0.08
	1.02	0.62	0.70	0.78	0.05	0.08
	0.83	0.38	0.74	0.71	0.03	0.06
	0.67	0.35	0.74	0.59	0.07	0.07
YZ	0.78	0.28	0.45	0.66	0.14	0.02
	0.88	0.56	0.59	0.73	0.11	0.08
	1.11	0.76	0.84	0.69	0.11	0.07
	0.91	0.70	0.71	0.67	0.11	0.01
	0.95	0.66	0.63	0.85	0.13	0.01
Average	0.89	0.54	0.66	0.69	0.09	0.05

**Table 2-5(b): Disc heights of SHAM IVD**

## **2.5 Conclusion:**

This study investigated whether the biomechanical performance of IVDs having anchored all sides by electrospun fiber mesh is comparable to natural and those IVDs made with silicone NP only. The short time (static) compression, rheological, finite element tests using human lumbar spine model showed the potentiality of the disc as a tissue-engineered IVD. The disc heights are also calculated for the IVD implanted in a rat tail and is observed that the average disc height remains same. Further long time (fatigue) biomechanical tests and finite element analysis are required to verify the feasibility of our electrospun fiber produced IVD to restore the biomechanical function native disc after discectomy. Also, histological analysis can be done to determine the bone growth around the implanted IVD.

## **2.6 Acknowledgements:**

This research was made possible by grant 8P20GM103447 from the US National Institutes of Health and on-campus faculty grant program from the University of Central Oklahoma Office of Research and Grants. Specifically, the research was possible from Mevlana Exchange Programme grant MEV 2016-097 from the Council of Higher Education (CoHE) in Turkey.

## **2.7 Future Works:**

A Histological analysis will be conducted on three different sets of samples which include the control set, sham (the existing IVD is completely taken out) and the engineered IVD. They will be stained with alcian blue for proteoglycans, picosirius red staining for collagen and hematoxylin and eosin.

## CHAPTER 3

### 3. THE IN-VIVO BIOLOGICAL RESPONSE OF NANOFIBER COATING ON A METAL IMPLANT

#### 3.1 Summary

Titanium-based alloy has been widely used in orthopedic and orthodontic surgeries as implants because of their strong mechanical, chemical (corrosion resistance), and biological properties and biocompatibility. [20] However, after implantations, patients are suffering from pain and the implant is taking nearly 7-8 years to get used to the human body. This study is based on the hypothesis that the titanium rod's biocompatibility can be increased by treating it with electrospun PCL nanofibers. To achieve this study, an implant grade titanium Ti-6AL-4V is taken and its surface has been modified before implantation. Grooves are made on the Ti rod using full spectrum laser. The grooves are of 100 microns in depth and 250 microns wide. The Ti rod is then treated with tesryl chloride for 48 hours followed by fibernectin for 24 hours to enhance the cell growth on the implant. The Ti rod is then sprayed with PCL nanofibers and treated with collagen. The sample is then implanted in the rabbit femur. After certain days of implantation, the rabbit is euthanized and the rabbit femurs are collected. The sample is fixed in 10% formalin for 48 hours and then it is cut into blocks of 7cm without disturbing the Ti implant. The samples are then dehydrated, pre-infiltrated and then polymerized using Technovit 7200 VLC. The samples are glued on to the slides using Technovit 7210 and Technovit 4000. Samples were grinded into a thin section of 25 – 30-micron thickness and then they are stained with Sanderson's red and blue stain to observe the cell growth around the Ti implant. It is observed that the bone growth around the modified Ti implant is increasing with a period of time. The rabbits

are euthanized on 14, 28 and 42 days after implantation and the samples are collected to observe the bone growth.

### **3.2 Background and Significance**

Ever since the evolution of metal implantation, Ti-6AL-4V (Titanium implant grade) is one the most used implants in the medical history because of its high strength, resistance to corrosion, bio-compatibility, and Osseointegration properties. As of today, there are approximately 1300 different implant systems which vary in shape, dimension, surface material and topography, wettability, surface chemistry and surface modification. [21] The surface characteristics like topography, wettability and coatings help in the Osseointegration of the implant. Improving the biocompatibility of an implant and to attain good osseointegration of the implants around the bone and surrounding tissue are important factors in the implantation. To improve the biomechanical efficiency and the Osseointegration of the titanium implant, it is grooved with laser for about 100 microns deep with spacing of 250 microns between each groove and then it is treated with tesryl chloride for 48 hours and fibernectin for 24 hours which bonds covalently and improve the attachment of cells on the surface. [19] The implant is then coated with electrospun nanofibers between the grooves to improve the cell growth around the implant and also the biomechanical efficiency.

### 3.3 Materials and Methods

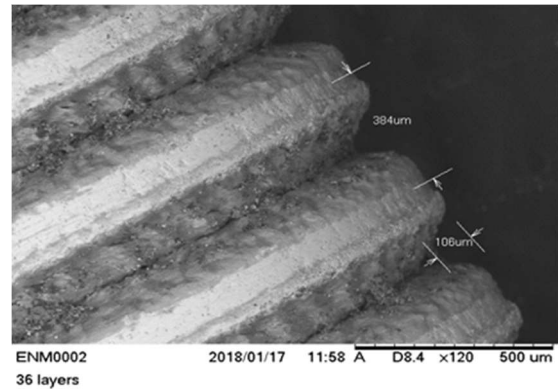
#### 3.3.1 Materials

The Titanium rods of implant grade Ti-6AL-4V are used. PCL pellets (pellet size ~3 mm, average  $M_n$  80,000) and acetone (laboratory reagent  $\geq 99.5\%$ ) were purchased from Sigma Aldrich (Sigma-Aldrich Co., LLC, St. Louis, MO, USA). Technovit 7200 VLC, Technovit 7210 and Technovit 4000 were purchased from EXAKT Technologies, Inc. (EXAKT Technologies, Inc. Broadway Extension Oklahoma City, OK 73116 – USA).

#### 3.3.2 Sample Fabrication Process



(a)



(b)

**Figure 3-1: (a) Laser grooving on the Ti surface using Full Spectrum Laser  
(b) SEM image of the implant**

#### (a) Grooving on the Ti implant

The Ti implant is first polished with three different polish papers and lubricants as shown in the figure. Then it is grooved using the full spectrum laser. An AutoCAD file is designed such that the depth of the groove on Ti implant is  $100\mu\text{m}$  and the gap between each groove is  $250\mu\text{m}$ . Then, the image of the implant is taken with Scanning Electron Microscopy

(SEM) to check the dimensions. The sample is cut into a desired length and then autoclaved.

(b) Surface modification of the Ti implant

After grooving, the Ti implant is treated with tesryl chloride and fibernectin. First, the implant is autoclaved and then it is dropped into a container of tesryl chloride (2,2,2-trifluoroeth- anesulfonyl chloride) for 48 hours. After 48 hours, it is transferred carefully into a vial containing plasma fibernectin of concentration 0.1mg/ml. [19]

(c) Nanofiber treatment and implantation:

Collagen is put on top of the implant and is fixed to the implant holder to spray fibers on the implant as shown in the Figure 3-2. It is then implanted in the femur of a rabbit. After 56 days of implantation, the rabbit is euthanized. Immediately after euthanization, the implants with the bone is fixed in 10% formalin.

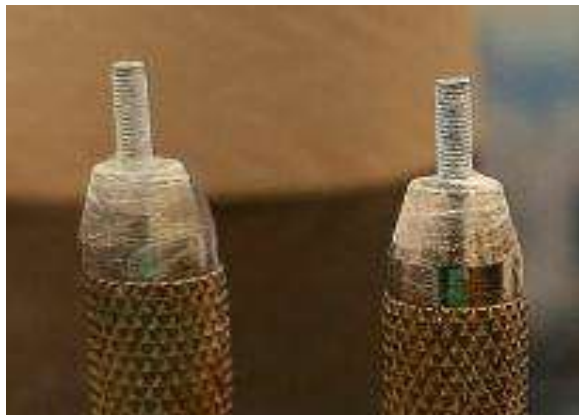


**Figure 3-2: The modified Ti samples are coated with PCL nanofibers, placed in a holder.**

(d) Fixation, dehydration, pre-infiltration, and polymerization of the sample for histological analysis:

The fresh sample is fixed in 10% neutral buffered formalin (NBF) and then it is dehydrated in a five-step process. The first step of dehydration starts by placing the sample in 70% ethanol and then followed by 80% ethanol, 96% ethanol and two different solutions of absolute ethanol. Each step is carried out for three days under agitation. After dehydration, the sample is pre-infiltrated using Technovit-7200 VLC. The pre-infiltration is carried out in four different steps starting with 30% Technovit-700 VLC in ethanol (3 days) and then with 50% (3 days), 70% (3 days) and finally with 100% Technovit-7200 VLC for 6-8 days under agitation. The pre-infiltration is done in a dark container because the Technovit-7200 VLC is a photosensitive material.

The sample is now ready for embedding in the blocks. Using the Light Polymerization Unit (LPU), the sample is embedded in the Technovit-7200 VLC solution. This solution solidifies when exposed to the blue and orange lights in the LPU. The samples are embedded in the Technovit 7200 VLC as shown in Figure 3-3. This process takes about 34 days after euthanizing the rabbit.



**Figure 3-3: The implant is embedded in the Technovit-7200 VLC**

After the samples are embedded, the blocks are glued on to the thin and thick plastic slides (Cadillac Plastic) using the adhesives Technovit-4000 and Technovit-7210. To maintain the parallelism between the two slides, precision adhesive press by EXAKT is used. The embedded sample is sandwiched between thick and thin slides as shown in the Figure 3-4. The EXAKT pathology saw is used to cut the sample for our area of interest and the slide is grinded using the EXAKT-CS 400. The sample is grinded to a thickness of 25-30 $\mu$ m.

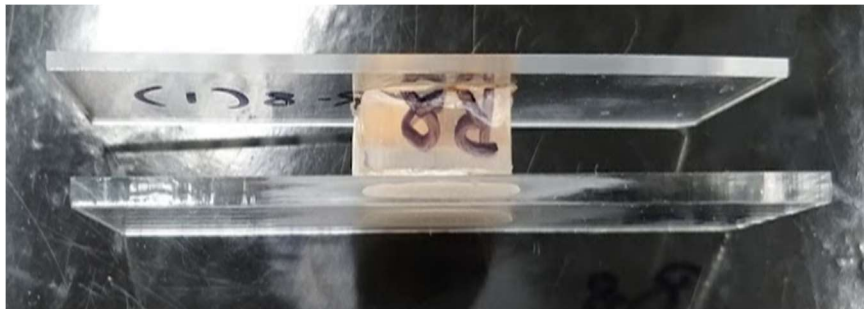


**Figure 3-4: The sample is sandwiched between a thick and thin plastic slide.**

### 3.3.3 Blood serum Collection:

The blood is collected from the rabbits on 0, 14, 28 and 42 days to analyze the serum for the analysis of Osteocalcine (OC), Alkaline phosphatase (ALP), and Tartrate-resistant acid phosphatase (TRAP). The OC, ALP, and TRAP determines the amount of bone formation and resorption in each of the sample. The osteocalcine and Alkaline phosphatase are supposed to be increasing with respect to time if the new bone is forming after the implantation and the Tartrate-resistant acid phosphatase should be decreasing slightly with time as the bone is forming. Thus, these three components in the blood are analyzed for bone formation and resorption using the Polymerase Chain reaction (PCR) kits.



### 3.3.4 μCT analysis:

To determine the amount of bone growth near the implant and in the grooves, μCT analysis is done. A line parallel to the grooves is drawn and the image is checked for the bone to implant contact value over a period of time as shown in Figure 3-5.



**Figure 3-5: The cell growth is counted in the highlighted area**

## 3.4 Results and Discussions

### 3.4.1 Histological Analysis

After embedding and sectioning the samples to a thickness of 25-30 microns, they are stained using the Sanderson's Rapid Bone Stain (RBS) of red and blue colored stains to determine the cell growth around the implant. The RBS is preheated to 55-60° C in an oven. The slide with the sample is dipped in the stain for 30 seconds. The excess stain can be removed using a laboratory wipe. This is followed by staining it with counterstain at room temperature with acidified acid fusion for 10-15 seconds. Now, depending on the color observed, we can determine the cell growth around the implant. With Acid fusion counterstain, if the color is pink it indicates the mineralized bone and osteoid indicates blue. For the Van Gieson counterstain, the mineralized bone will be in yellow-orange, osteoid is in blue-green color while the cells in the bone marrow are blue in color. The implants are categorized into three different sample size: 14 days, 28 days and 42 days depending on the euthanization of a rabbit after implantation. The Figure 3-5 shows the cell growth over a period of time.

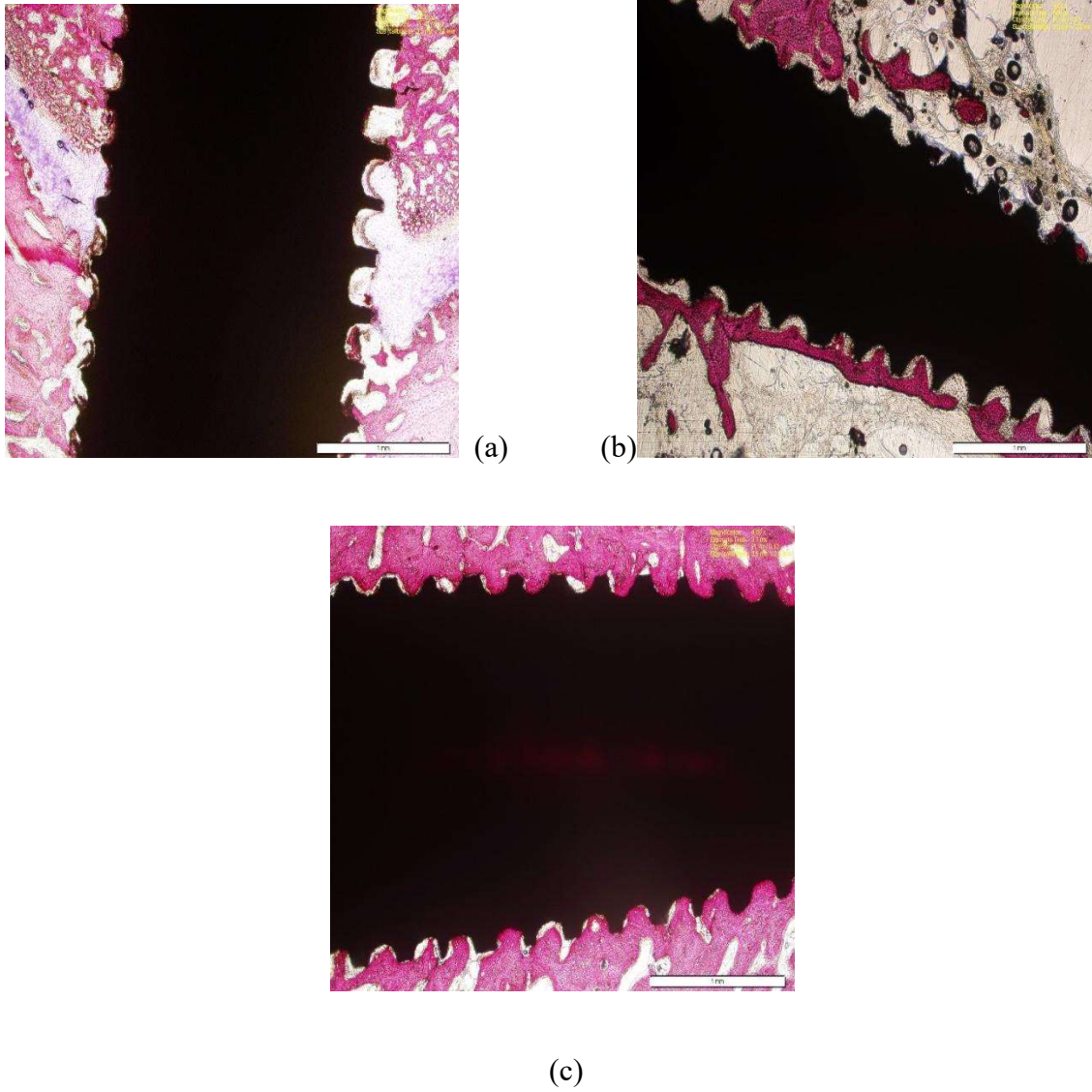


**Figure 3-6: Showing the cell growth after (a) 14 days (b) 28 days (c) 42 days after implantation**

#### 3.4.2 Bone formation and resorption:

Using the Polymerase Chain Reaction (PCR) kit, a graph is plotted for the amount of Osteocalcine, Alkaline Phosphate, and Tartrate-resistant acid phosphate (TRAP) present in the serum marker concentration (ln) for different sets of samples. The results show the bone formation and resorption in the Figure 3-6.

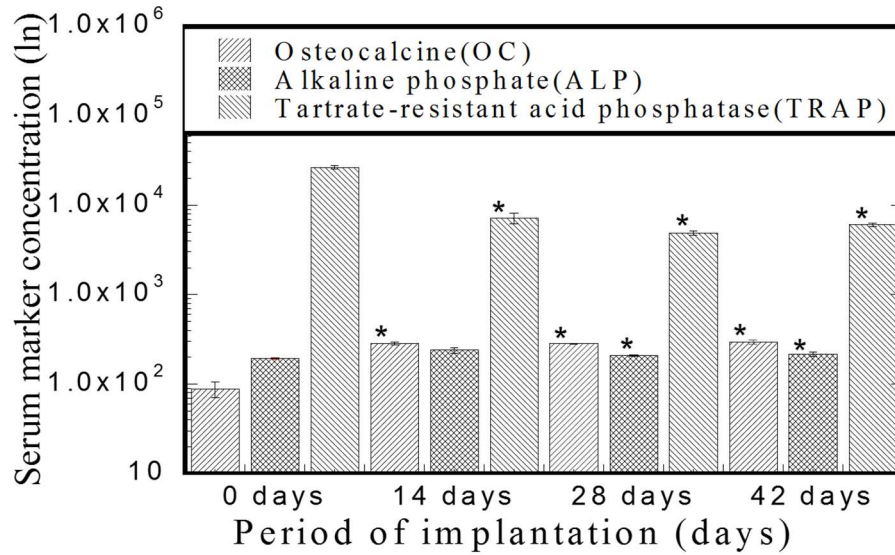


**Figure 3-7: Amount of OC, ALP, and TRAP present in the serum concentration over a period of implantation**

### 3.4.3 μCT analysis:

The bone to implant contact value is calculated over the period of implantation of the sample i.e., for 14 days, 28 days and 42 days. For the 14 days implant, the mean voxel value is around 380 and is found to be increasing for 28 days and 42 days to 520 and 540 respectively as shown in the Figure 3-8.

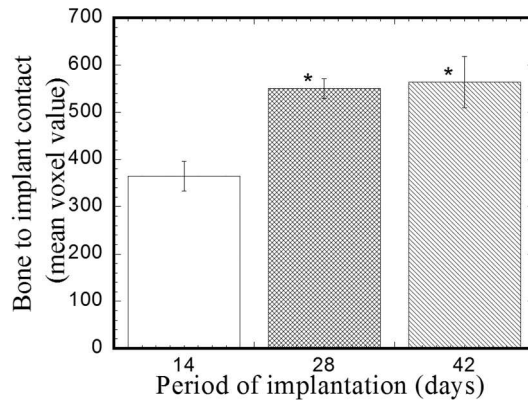


**Figure 3-8: Graph plotted for mean voxel value for period of implantation.**

### **3.5 Conclusion:**

From the above results, we can conclude that the cell growth around the Titanium implant can be done by surface modifications of the implant and PCL nanofibers enhances the cell growth. Further studies can be done to determine the types of cells around the implant.

### **3.6 Acknowledgments:**

I would like to acknowledge Dr. Amal Shediwah and Sadegh Nikfarjam for their support and contribution throughout the research.

### **3.7 Future Works:**

The samples can be further processed to determine the type of cell growth around the Titanium implant. Also, the amount of bone to implant contact (BIC) value can be determined.

## CHAPTER 4

### 4. DESIGN AND FABRICATION OF A BLOOD VESSEL

#### 4.1 Summary:

The onerous challenge of the tissue engineering is to produce small diameter blood vessels. Typically, an engineered blood vessel construct made with compliant tubular core and the circumference is covered with fibrous material. The inside of the core can be made of hydrogel, where the outside can be made with nanofibers. Nano fibrous materials have the potential to grow new blood vessels. Nylon-6 is a good biomaterial that can be used to fabricate a blood vessel. In this study, a blood vessel is fabricated using Nylon-6 and is tested for the fluid flow.

#### 4.2 Background and Significance:

People diagnosed with peripheral arterial diseases or those who've just received a transplant have a benefit from the engineered blood vessel. [22] Recent advances in nanotechnology and increasing recognition of the potential of Nano materials as biocompatible and biomimetic scaffolds for cells have provided new tools for tissue engineering and the development of three-dimensional (3D) cell cultures. [23] In recent years, there are different processing techniques to prepare nano fibers to produce vascular grafts. [24] Some of the techniques are, template synthesis, phase separation, drawing, self-assembly, electrospinning etc. According to Zheng-Ming Huang [25], the electrospinning process is the only method, which can be further developed for mass production of one-by-one continuous nanofibers from various polymers. [26] Electrospinning is a fiber

production method which uses electric force to draw charged threads of polymer solutions or polymer melts up to fiber diameters in the order of some hundred nanometers. [27]

#### **4.3 Materials and Methods:**

Nylon-6, in the form of pellets and Formic Acid (reagent grade,  $\geq 95\%$ ) are bought from Sigma-Aldrich. Formic Acid is used as a solvent to prepare a Nylon-6 polymer solution. Formic Acid is diluted with distilled water to 88% and is mixed with Nylon-6 pellets in the 10% w/w ratio. To obtain a homogeneous mixture of the solution, it is sonicated at 60% frequency for 45 minutes. The solution is then applied on to a metal rod which rotates at a certain rpm to hold the solution in place. After 10 minutes of exposing the metal rod to air, the Nylon-6 polymer solution solidifies. It is quenched with water. The Nylon-6 fiber can be removed from the metal rod and a cylinder with hollow faces is obtained which looks like a tube. The fabricated blood vessel is shown in the Figure 4-1.



**Figure 4-1: Blood vessel fabricated by Nylon-6**

## 4.4 Results and Discussion:

### 4.4.1 Flow Test:

The fabricated blood vessel is tested for the flow using the variable flow meter as shown in Figure 4-2. The blood vessel is connected with two needles which have the same outer diameter as the inner diameter of the blood vessel at two ends. These needles are connected to pipes which go into the water reservoir as shown in the Figure 4-3. The flow test is carried out by passing water at different flow rates. For a maximum flow rate of 100ml/min, we could not see any leakage from the blood vessel.



**Figure 4-2: A mini variable Flow Pump**



**Figure 4-3: Flow test setup for a fabricated blood vessel**

#### 4.4.2 Rupture test:

On the other hand, the water is pumped into the blood vessel from one end and the other end of the tube is closed to see if the blood vessel ruptures due to the pressure created by the fluid. Surprisingly, the blood vessel didn't break or leak and the variable flow pump stopped pumping the fluid anymore. The water level in the reservoir remained same.

#### 4.4.3 Tensile Test:

The tensile strength of the Nylon-6 is tested using the Universal Test Resources machine. The two ends of the blood vessel are fixed in the vice of the Test Resources equipment as shown in the Figure 4-4 (a). Then the moving vice is raised upwards slowly at a rate of 0.05m/s. As soon as the blood vessel breaks, the vice raises up completely as shown in Figure 4-4 (b).





(a)



(b)

**Figure 4-4: (a) The blood vessel is fixed between two jaws of the Test Resources machine (b) Breaking of the fabricated blood vessel**

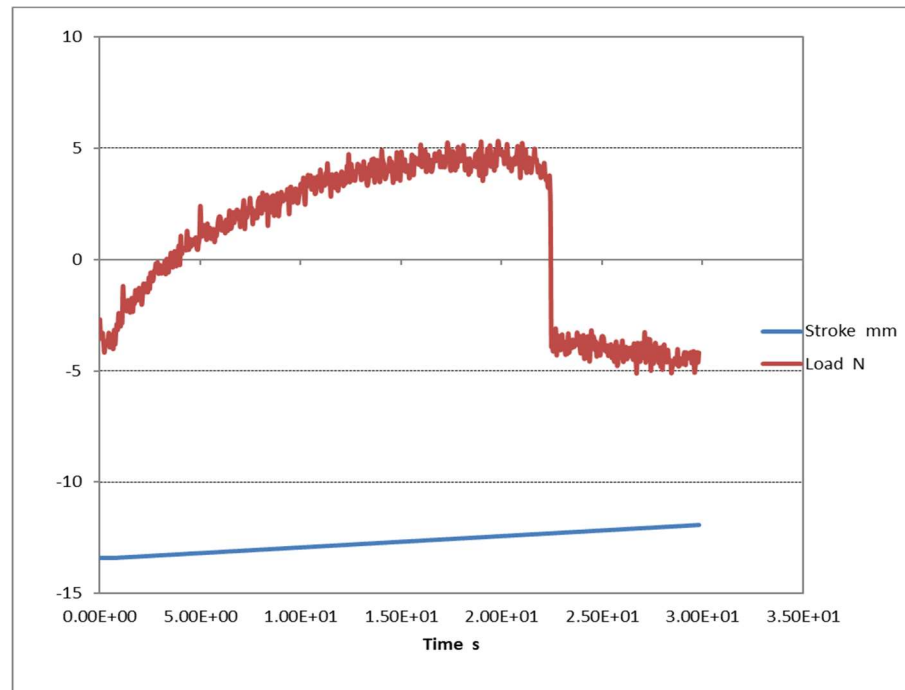


**Figure 4-5: Graph plotted to determine tensile strength with Time(s) on X-axis and Load (N) and Stroke (mm) on Y-axis**

Using the Test Resources software, a graph can be plotted and the maximum tensile strength can be determined. The tensile strength is found to be 10N. The graph is plotted using the data with Load (N) and Stroke (mm) vs Time(s) as shown in the Figure 4-5.

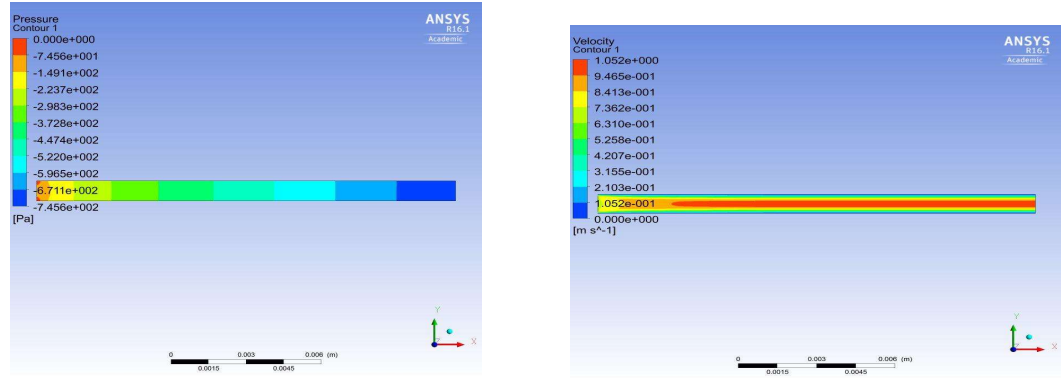
#### 4.4.4 ANSYS Simulation:

The dimensions of the blood vessel are measured using the Scanning Electron Microscopy (SEM). The flow of blood is simulated in Ansys Fluent using the properties of blood and the velocity is calculated using the maximum shear stress of the blood vessel of 60 dynes/cm<sup>2</sup>. [27]

Using the maximum wall shear stress of a blood vessel, the flow rate is calculated using,

$$\tau = 32 * \mu * \frac{Q}{\pi d^3} [27]$$

From the flow rate, the maximum velocity in a blood vessel is calculated and found to be 0.72 m/s. The viscosity ( $\mu$ ) of the blood is considered as 0.00287 kg/m/s and the density is taken as 1060 kg/m<sup>3</sup>. The contours are plotted for pressure and velocity as shown in the Figure 4-6. The flow of the blood is taken as laminar and the axis is considered as axis-symmetric on the design. The simulation is done for a no-slip condition on the walls of the blood vessel.



(a)

(b)

**Figure 4-6: The contours of (a) Pressure and (b) Velocity of a simulated blood vessel**

#### **4.5 Conclusion:**

This study investigated if a blood vessel can be fabricated using the Nylon-6 polymer and flow tests are conducted to determine if it sustains the maximum flow of blood without rupture or leaking. The tensile strength of the blood vessel is also determined using the Test Resources equipment and the blood flow is simulated using the ANSYS fluent software.

#### **4.6 Acknowledgements:**

I would like to acknowledge Dr. Mohammed Hossan for his invaluable insights in achieving the goal.

#### **4.7 Future Works:**

Using this preliminary study, the blood vessel can be further modified to make it more biocompatible and its tensile strength can be further increased by adopting conventional nanofiber producing techniques like electrospinning.

## References:

1. Lennon, A.B., B.A.O. McCormack, and P.J. Prendergast, *The relationship between cement fatigue damage and implant surface finish in proximal femoral prostheses*. Medical Engineering and Physics, 2003. **25**(Compendex): p. 833-841.
2. Baker, S.R., et al., *Determining the mechanical properties of electrospun poly-ε-caprolactone (PCL) nanofibers using AFM and a novel fiber anchoring technique*. Materials Science and Engineering: C, 2016. **59**: p. 203-212.
3. Huglin, M.R., *Hydrogels in medicine and pharmacy Edited by N. A. Peppas, CRC Press Inc., Boca Raton, Florida, 1986 (Vol. 1), 1987 (Vols 2 and 3). Vol. 1 Fundamentals, pp. vii + 180, £72.00, ISBN 0-8493-5546-X; Vol. 2 Polymers, pp. vii + 171, £72.00, ISBN 0-8493-5547-8; Vol. 3 Properties and Applications, pp. vii + 195, £8000, ISBN 0-8493-5548-6*. British Polymer Journal, 2007. **21**(2): p. 184-184.
4. Peppas, N.A., et al., *Hydrogels in pharmaceutical formulations*. Eur J Pharm Biopharm, 2000. **50**(1): p. 27-46.
5. Fett, T., *Stress intensity factors for edge-cracked plates under arbitrary loading*. Fatigue & Fracture of Engineering Materials & Structures, 1999. **22**(4): p. 301-305.
6. Lee, K.Y. and D.J. Mooney, *Hydrogels for tissue engineering*. Chemical Reviews, 2001. **101**(7): p. 1869-1879.
7. Bosworth, L.A., L.A. Turner, and S.H. Cartmell, *State of the art composites comprising electrospun fibres coupled with hydrogels: a review*. Nanomedicine, 2013. **9**(3): p. 322-35.

8. Yasar, O., et al., *Mechanical Characterization of Polyethylene Glycol Diacrylate (PEGDA) for Tissue Engineering Applications*, in *Mechanics of Biological Systems and Materials, Volume 5*, B.C. Prorok, et al., Editors. 2013, Springer New York. p. 189-195.
9. Chen, F., et al., *Preparation and characterization of oxidized alginate covalently cross-linked galactosylated chitosan scaffold for liver tissue engineering*. *Materials Science and Engineering: C*, 2012. **32**(2): p. 310-320.
10. Azartash-Namin, K., et al., *Mechanical Effectiveness of Polyvinyl Alcohol/Polyvinyl Pyrrolidone (PVA/PVP) as an Intervertebral Disc Polymer*. Vol. 3. 2013.
11. Available from: <http://clinicalgate.com/intervertebral-disc-process-of-degeneration-physiology-and-pathophysiology/>.
12. Gloria, A., et al., *Dynamic-mechanical properties of a novel composite intervertebral disc prosthesis*. *J Mater Sci Mater Med*, 2007. **18**(11): p. 2159-65.
13. Nerurkar, N.L., et al., *Engineered disc-like angle-ply structures for intervertebral disc replacement*. *Spine (Phila Pa 1976)*, 2010. **35**(8): p. 867-73.
14. Martin, J.T., et al., *Translation of an engineered nanofibrous disc-like angle-ply structure for intervertebral disc replacement in a small animal model*. *Acta Biomater*, 2014. **10**(6): p. 2473-81.
15. Vadalà, G., et al., *Bioactive electrospun scaffold for annulus fibrosus repair and regeneration*. *European spine journal : official publication of the European Spine Society, the European Spinal Deformity Society, and the European Section of the Cervical Spine Research Society*, 2012. **21 Suppl 1**: p. S20-6.

16. Attia, M., J.P. Santerre, and R.A. Kandel, *The response of annulus fibrosus cell to fibronectin-coated nanofibrous polyurethane-anionic dihydroxyoligomer scaffolds*. *Biomaterials*, 2011. **32**(2): p. 450-60.
17. Khandaker, M. and S. Riahinezhad. 06/21/2016: United States of America.
18. Shin, D.S., K. Lee, and D. Kim, *Biomechanical study of lumbar spine with dynamic stabilization device using finite element method*. *Computer-Aided Design*, 2007. **39**(7): p. 559-567.
19. Ueno, K. and Y.K. Liu, *A three-dimensional nonlinear finite element model of lumbar intervertebral joint in torsion*. *J Biomech Eng*, 1987. **109**(3): p. 200-9.
20. Brunette, D.M., et al., *Titanium in Medicine: Material Science, Surface Science, Engineering, Biological Responses and Medical Applications*. 1 ed. Engineering Materials. 2001.
21. Junker, R., et al., *Effects of implant surface coatings and composition on bone integration: a systematic review*. *Clin Oral Implants Res*, 2009. **20 Suppl 4**: p. 185-206.
22. Correia, T.R., et al., *Development of UV cross-linked gelatin coated electrospun poly(caprolactone) fibrous scaffolds for tissue engineering*. *Int J Biol Macromol*, 2016. **93**(Pt B): p. 1539-1548.
23. Ge, J., et al., *The size of mesenchymal stem cells is a significant cause of vascular obstructions and stroke*. *Stem Cell Rev*, 2014. **10**(2): p. 295-303.
24. Zhao, X., et al., *3D patterned substrates for bioartificial blood vessels - The effect of hydrogels on aligned cells on a biomaterial surface*. *Acta Biomater*, 2015. **26**: p. 159-68.

25. Carlton, R.J., et al., *Chemical and biological sensing using liquid crystals*. *Liq Cryst Rev*, 2013. **1**(1): p. 29-51.
26. Khan, M., et al., *A liquid-crystal-based DNA biosensor for pathogen detection*. *Scientific Reports*, 2016. **6**: p. 22676.
27. Papaioannou, T.G. and C. Stefanadis, *Vascular wall shear stress: basic principles and methods*. *Hellenic J Cardiol*, 2005. **46**(1): p. 9-15.